THE JOURNAL OF PHYSICAL CHEMISTRY B

Article

pubs.acs.org/JPCB

Understanding SO_2 Capture by Ionic Liquids

Anirban Mondal and Sundaram Balasubramanian*

Chemistry and Physics of Materials Unit, Jawaharlal Nehru Centre for Advanced Scientific Research, Bangalore 560 064, India

Supporting Information

ABSTRACT: Ionic liquids have generated interest for efficient SO_2 absorption due to their low vapor pressure and versatility. In this work, a systematic investigation of the structure, thermodynamics, and dynamics of SO_2 absorption by ionic liquids has been carried out through quantum chemical calculations and molecular dynamics (MD) simulations. MP2 level calculations of several ion pairs complexed with SO_2 reveal its preferential interaction with the anion. Results of condensed phase MD simulations of SO_2–IL mixtures manifested the essential role of both cations and anions in the solvation of SO_2, where the solute is surrounded by the "cage" formed by the cations (primarily its alkyl tail) through dispersion interactions. These structural effects of gas absorption are substantiated by calculated Gibbs free energy of solvation; the dissolution is demonstrated to be enthalpy driven. The entropic loss of SO_2 absorption in ionic liquids with a larger anion such as $[NTf_2]^-$ has been quantified and has been attributed to the conformational restriction of the anion imposed by its interaction with SO_2. SO_2 loading IL decreases its shear viscosity and enhances the electrical conductivity. This systematic study provides a molecular level understanding which can aid the design of task-specific ILs as electrolytes for efficient SO_2 absorption.

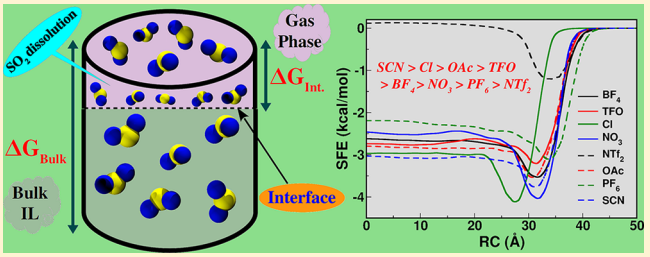

INTRODUCTION

Sulfur dioxide (SO_2), a dominant air pollutant, is released into the atmosphere through the combustion of fossil fuels for energy conversion. For instance, the gas emission from coal plants contains 0.3–5% of SO_2.[1] It is extremely important to control and minimize this outflow, as it is harmful to environment and causes health hazards.[1]

Another important aspect concerning SO_2 is its use as a component in lithium–sulfur dioxide (Li–SO_2) batteries.[2] Li–SO_2 system is a class of primary battery which is longer-lasting than alkaline ones, metal-air batteries etc., with high energy density, wherein the inexpensive SO_2 can be used as the active cathode material.[3] Also, Li–SO_2 battery has some inherent advantages in contrast to other primary batteries, such as alkaline batteries,[4] and metal-air batteries;[5] for instance, Li–SO_2 battery has a high energy density (up to 330 Wh kg^{-1}, i.e., 2–4 times higher than those of alkaline batteries) and good discharge performance with working voltage around 3.0 V.[2] These unique characteristics have made Li–SO_2 batteries to be useful for applications requiring long service life which is beyond the reach of conventional primary batteries.

In spite of these positive attributes, safety issues associated with Li–SO_2 batteries restrict its applications;[3] the cell is comprised of liquefied SO_2 under pressure, and this constrains the upper limit of pressure that it can resist without leaking toxic SO_2, being 3.4 atm at 294 K.[2] Moreover, the electrolyte, acetonitrile being used in a Li–SO_2 battery is volatile in nature and can lead to an uncontrolled increase in pressure, resulting in the risk of fire. A great deal of effort has focused on the search for electrolyte solvents which have low vapor pressure, and are less reactive too.[6,7]

In light of these facts, there is general interest to develop new materials for the efficient, reversible, and economical capture of SO_2 which can also function as electrolytes. Traditional technologies developed over the years for flue-gas desulfurization (FGD) includes limestone scrubbing, ammonia scrubbing, and absorption by organic solvents.[8,9] As an alternative, ionic liquids (ILs) have manifested their efficacy as better absorbents for acidic gases such as SO_2,[10−13] and CO_2,[14−18] owing to their properties such as low vapor pressure, high thermal and chemical stability, wide liquid temperature range, nonflammability, and tunable properties.[19−21] Three types of interactions such as physical, chemical or hybrid (physical and chemical), play important roles in the solubility of SO_2 in ILs.[12,16,22−24] However, an effective capture of SO_2 from flue gases entails chemical absorption because of low partial pressure in flue gases.[25] Han et al. demonstrated the first example of SO_2 capture by chemisorption in a functionalized IL, namely, tetramethylguanidinium lactate ([TMG][L]).[10] Subsequently, several other functionalized ILs were explored for effective SO_2 capture, including hydroxyl ammonium ILs,[26] imidazolium ILs,[22,23,27−29] TMG-based ILs,[12] phenolate-based ILs,[30] and supported ionic liquid membranes (SILMs).[31−33] In general, the chemisorption of SO_2 is based on strong interactions between SO_2 with the electronegative oxygen atom or nitrogen atom in the anion.[24,34,35] Recently, a new strategy was developed for improving SO_2 capture through multiple-site

Received: March 11, 2016
Revised: April 27, 2016
Published: April 27, 2016

DOI: 10.1021/acs.jpcb.6b02553
J. Phys. Chem. B 2016, 120, 4457−4466

absorption by tunable ILs.[36−40] In the current manuscript, we examine the physical adsorption of SO_2 in imidazolium ILs.

The observed trend of SO_2 solubility in ionic liquids from experimental measurements are not entirely conclusive. Jiang et al. reported the solubility of SO_2 in imidazolium based ILs in the order $[BMIM][BF_4] > [BMIM][NTf_2] > [BMIM][PF_6]$ at 298 K and 1 bar.[31] In another study, the order in SO_2 solubility in $[BMIM]^+$ based ILs was seen to be $[OAc]^- > [NTf_2]^- > [BF_4]^- > [PF_6]^-$.[41] In a recent work, Dai and co-workers reported the SO_2 solubility in imidazolium ILs in the following order, $[SCN]^- > [Cl]^- > [NTf_2]^-$ at 296 K and 1 atm.[2]

Molecular simulations are frequently employed to understand microscopic interactions. In recent years, several molecular simulation studies to understand gas absorption in ILs have been undertaken.[42−57] Maginn et al. explored the effect of anion on the high solubility of CO_2 in imidazolium based ILs by molecular dynamics (MD) simulations.[42] Ribeiro et al. investigated the structure and dynamics of 1-butyl-3-methylimidazolium bromide ([BMI][Br]) IL on addition of SO_2 using MD simulations and Raman spectroscopy.[58] Wick and co-workers employed a polarizable force field to examine the binding of CO_2 and SO_2 at the air/liquid interface of 1-butyl-3-methylimidazolium tetrafluoroborate ([BMIM]-$[BF_4]$).[59] A minimum in free energy was observed at the interface. The nature of interactions between acidic gases at the interface of ILs was further studied using Gibbs free energy of solvation by many research groups.[60,61]

As mentioned above, most studies have focused on interactions in CO_2−IL mixtures, while only a few have been devoted to SO_2−IL mixtures.[59,61,62] Furthermore, a systematic study of interactions of SO_2 at IL interface and its anion dependence is lacking. Needless to state, a fundamental understanding of interactions between ILs and SO_2 is extremely important for the further design of new ILs for SO_2 absorption. The present work is aimed in this direction and examines the anion dependence of SO_2 capture in eight ionic liquids using MD simulations and quantum chemical calculations. On the basis of the solvation free energy and binding energies of SO_2 in ILs, we find the IL with the thiocyanate anion to be the most suited for SO_2 absorption.

COMPUTATIONAL DETAILS

ILs, all having 1-butyl-3-methylimidazolium ($[BMIM]^+$) as the cation, and the following anions, chloride ($[Cl]^-$), nitrate ($[NO_3]^-$), tetrafluoroborate ($[BF_4]^-$), hexafluorophosphate ($[PF_6]^-$), triflate ($[CF_3SO_3]^-$), bis(trifluoromethanesulfonyl)-imide ($[NTf_2]^-$), acetate ($[OAc]^-$), and thiocyanate ($[SCN]^-$) were studied. These are displayed in Figure 1. The atom labeling in $[BMIM]^+$ cation is shown in Figure 2. Three different approaches were utilized to study SO_2−IL interactions: (i) quantum chemical (QM) calculations, (ii) classical molecular dynamics (MD) simulations, and (iii) free energy (FE) calculations based on point ii.

QM Calculations. Systems, each of isolated IL ion pair, SO_2 molecule, and SO_2−IL complex (one SO_2 molecule and one IL ion pair) were geometry optimized at MP2/aug-cc-pVDZ level of theory. Five different initial configurations were constructed using GaussView software,[63] wherein the SO_2 molecule was kept near H_A, H_B, or H_1 sites. Optimized minima on the potential energy surface were confirmed via frequency analysis. Binding energy (BE) was estimated as the energy difference between the complex and the sum of the energy of components.

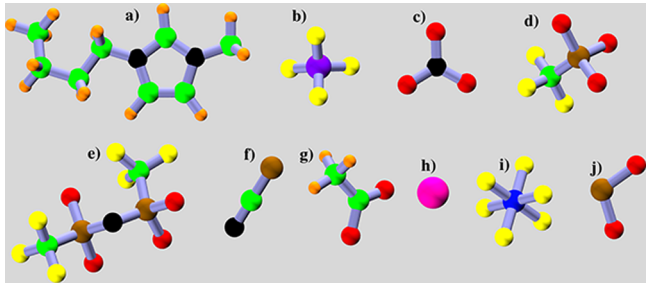

Figure 1. Molecular structure of (a) $[BMIM]^+$, (b) $[BF_4]^-$, (c) $[NO_3]^-$, (d) $[CF_3SO_3]^-$ or $[TFO]^-$, (e) $[NTf_2]^-$ or $[TFSO]^-$, (f) $[SCN]^-$, (g) $[CH_3COO^-]$ or $[OAc]^-$, (h) $[Cl]^-$, (i) $[PF_6]^-$, and (j) $[SO_2]$ used in simulations. Color scheme: nitrogen, black; carbon, green; hydrogen, orange; oxygen, red; sulfur, ochre; boron, violet; fluorine, yellow; phosphorus, blue; chlorine, magenta.

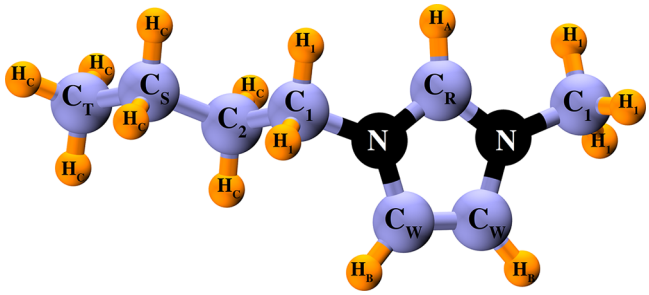

Figure 2. Atom labeling in $[BMIM]^+$ (1-butyl-3-methylimidazolium) cation.

$$BE = E_{SO_2-IL} - (E_{IL} + E_{SO_2}) \quad (1)$$

where E_{SO_2-IL}, E_{IL}, and E_{SO_2} represent energy of SO_2−IL complex, isolated IL ion pair with lowest energy and SO_2, respectively. Counterpoise corrections for basis set superposition error (BSSE) were added to the computed interaction energy.[64] The calculations were performed using Gaussian 09 program.[65] In rest of the discussion, we limit ourselves to that optimized configuration which had the best binding energy for SO_2.

To quantify the charge transfer in these SO_2−IL complexes, atomic site charges were computed using the DDEC/c3 method in gas phase.[66,67] To this end, minimum energy configurations were utilized to calculate the valence electron density of these systems and the same was employed as an input to DDEC/c3.

Classical Simulations. MD simulations were carried out with the LAMMPS program.[68] ILs were modeled using a nonpolarizable all-atom force field developed earlier within our group.[69−71] Interaction parameters for SO_2 were adopted from the work of Potoff et al.,[72] which was used previously to simulate SO_2 in ILs.[61] The parameters for cross-terms were computed by Lorentz−Berthelot rules. Particle−particle particle mesh solver was employed to evaluate the long-range electrostatic interactions. Equations of motion were integrated using velocity Verlet algorithm with a time step of 1 fs. Tail corrections to energy and pressure were applied. All C−H covalent bonds were constrained using SHAKE algorithm as implemented in LAMMPS.[68] The temperature and pressure in simulations were controlled using Nosé−Hoover thermostat[73,74] and barostat.

DOI: 10.1021/acs.jpcb.6b02553
J. Phys. Chem. B 2016, 120, 4457−4466

The initial configurations were generated with the program Packmol.[75] Experimental observations suggest that SO_2 is soluble in all ILs studied here up to at least 0.5 mol fraction at 298 K. Thus, the simulations of bulk solutions were performed in a cubic box containing 256 cations, 256 anions, and 128 SO_2 molecules to obtain a molar ratio of 0.5. Simulations were carried out at 298 K in order to compare the results against reported experimental properties (although [BMIM][Cl] is solid at 298 K, the simulations for SO_2 loaded [BMIM][Cl] system was also performed at 298 K for the sake of comparison). All the systems were equilibrated in the *NPT* ensemble for 10 ns duration. It was followed by another 5 ns equilibration in the *NVT* ensemble. Finally, a 48 ns production run was generated in the *NVT* ensemble. The simulated box dimensions for all SO_2−IL mixtures are tabulated in Table S1 of Supporting Information. For purpose of comparison, a separate simulation was performed with CO_2 loaded ionic liquid system at 298 K. The systems were visualized in VMD.[76]

Transport properties such as self-diffusion coefficient, shear viscosity and electrical conductivity were calculated using equilibrium Green−Kubo relations discussed earlier.[70,77]

Free Energy Calculations. All the FE simulations were carried out employing the colvars module[78] as implemented in LAMMPS.[68] The solvation free energy (SFE) can be defined as the energy required to bring one SO_2 molecule into bulk IL from the gas phase. A simulation cell containing 256 ion pairs was equilibrated in the *NPT* ensemble at 298 K for 8 ns ([BMIM][Cl] at 353 K, as it is a solid at room temperature). To create a liquid−vapor interface, the cell length along *z*-axis was stretched to 200 Å, and then the system was further equilibrated in the *NVT* ensemble for 2 ns. This was followed by FE calculations in the *NVT* ensemble. Colvar style "distance Z" was employed in determining the free energy profile using the adaptive biasing force (ABF) method.[79] The distance between the center of mass (COM) of IL molecules and the center of mass of SO_2 molecule was used to define the reaction coordinate (RC) (see Figure S1 of the Supporting Information). Four nonoverlapping windows along the *Z* direction were created to divide the whole reaction coordinate, spanning from 0 to 50 Å. The first and last window represents SO_2 to be completely submerged in bulk IL and completely in gas phase, respectively. ABF forces were applied every 500 steps with a bin width of 0.1 Å. In each window, an average sampling ratio of 5 between the highest and lowest point was achieved, after running for at least 40 ns.

RESULTS AND DISCUSSION

Quantum Chemical Analysis. The computed binding energies (BE) at MP2/aug-cc-pVDZ level of theory for SO_2−IL complexes are tabulated in Table 1. Aparicio et al. investigated the interaction strength in a pool of SO_2−IL systems by decomposing the total BE into cation−anion, SO_2−cation, and SO_2−anion contributions.[51] They observed SO_2−anion interactions to be the major contribution to total BE for SO_2−IL systems. In our calculations, BE varies between −31.38 kJ/mol ([BMIM][NTf_2]) and −82.19 kJ/mol ([BMIM][SCN]) (see Table 1).

Among the systems studied, there appears to be more than one approach for the SO_2 molecule to interact with the IL ions. Anions such as $[Cl]^-$ or $[SCN]^-$, prefer to be located above the imidazolium ring plane whereas SO_2 interacts along the C_1 site on cation. However, anions like $[BF_4]^-$, $[NO_3]^-$, and $[TFO]^-$, interact along the most acidic site on cation (C_R) and SO_2 prefers to stay above the ring plane, interacting with H_1 hydrogens. In the acetate system, both the anion as well as SO_2 prefer to be in the same plane as that of the imidazolium ring; while acetate anion shows very strong interaction with the acidic proton (H_A), SO_2 interacts with H_1 sites. But, in systems such as $[PF_6]^-$ and $[TFSO]^-$, SO_2 and the anion are located on either side of the imidazolium ring, resulting in minimal SO_2−anion interaction among all SO_2−IL system examined here. The same can be seen in the BE values for SO_2−IL system having either $[PF_6]^-$ or $[TFSO]^-$. The minimum energy structures of SO_2−IL complexes are displayed in Figure 3 and Figure S2 of Supporting Information.

Table 1. BSSE Corrected Binding Energies (BE) of SO_2−Ion Pair Systems at the MP2/aug-cc-pVDZ Level of Theory

SO_2−IL system	BE (kJ mol^{-1})
[BMIM][SCN]	−82.19
[BMIM][Cl]	−72.17
[BMIM][OAc]	−59.12
[BMIM][CF_3SO_3]	−57.78
[BMIM][NO_3]	−54.68
[BMIM][BF_4]	−49.51
[BMIM][PF_6]	−40.05
[BMIM][NTf_2]	−31.38

Charge transfer between SO_2 and IL has been reported earlier,[51] which can be used to understand the gas absorption capacity. The charge transfer between the ion pair and SO_2 molecule is calculated as the difference in total charge on SO_2 molecule in the isolated state and in the SO_2−IL complex and the same is tabulated in Table S2 of Supporting Information. In all the systems studied here, the total charge on SO_2 molecule is negative; this implies that charge is transferred to the SO_2 molecule from the ion pair. A linear relationship between the BE and charge transfer in these complexes is observed (Figure 4). The trend in observed experimental solubility[2,31,41] ties with that of the BE and points to the enthalpic nature of SO_2 solvation in ILs.

Liquid Structure. To obtain an insight into the effect of SO_2 on the structure of ILs, we compared cation−anion and anion−H_A radial distribution functions (RDFs) in the pure IL and in SO_2 loaded ILs (see Figure S3 of the Supporting Information). No significant changes were observed in these pair correlation functions upon SO_2 inclusion, which is consistent with previous MD simulations of SO_2 loaded ILs.[56,57,80] SO_2 solvation in ILs was further investigated through RDFs between the center of mass (COM) of the ions and that of SO_2 and the same are shown in Figure S4a of the Supporting Information and Figure 5. Anions interact with the solute better than cations do. Within its first coordination sphere, the SO_2 molecule is surrounded by around 1.5 anions and 5.5 cations (see Table S3 of the Supporting Information). The presence of such high cation to anion ratio (which was also seen in many instances for CO_2 solvation in ILs,[81,82] as well as for SO_2 solvation in [EMIM][SCN] from an *ab initio* MD study[57]) suggests a possible formation of "cation cage" around SO_2. Thus, it is worth investigating in more detail the role of contributing sites and compare them against results for CO_2 solvation by ILs.

We have examined various site−site RDFs to unveil the role of specific interactions in SO_2 solvation and these are displayed in Figure 6 and Figure S4b of the Supporting Information. The cation hydrogen atoms, e.g., H_B and H_1 possess a stronger

DOI: 10.1021/acs.jpcb.6b02553
J. Phys. Chem. B 2016, 120, 4457−4466

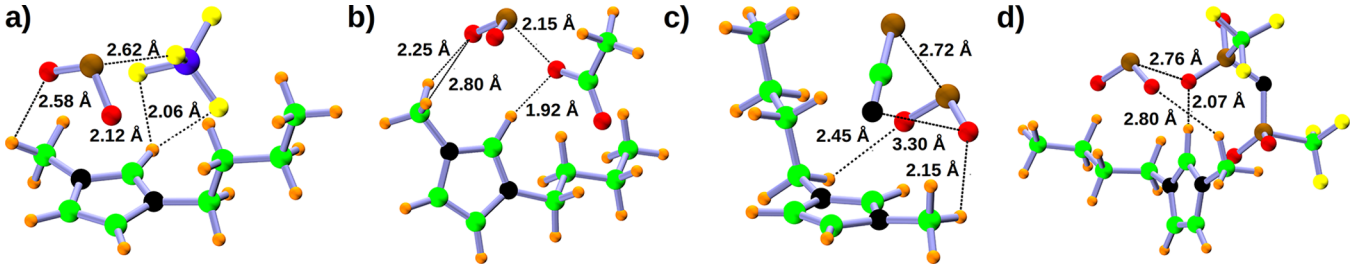

Figure 3. Minimum energy structures of SO_2–IL complexes at MP2/aug-cc-pVDZ level of theory: (a) [BMIM][BF_4], (b) [BMIM][OAc], (c) [BMIM][SCN], and (d) [BMIM][NTf_2]. Other structures are displayed in Figure S2 of Supporting Information.

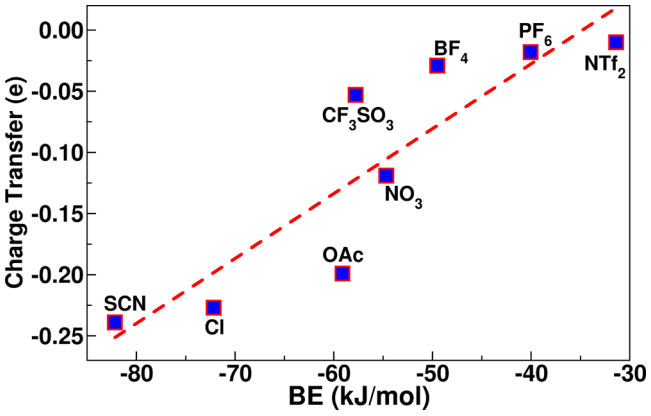

Figure 4. Binding energies versus charge transfer to SO_2 upon complexation with IL ion pairs in gas phase. $[BMIM]^+$ is the common cation.

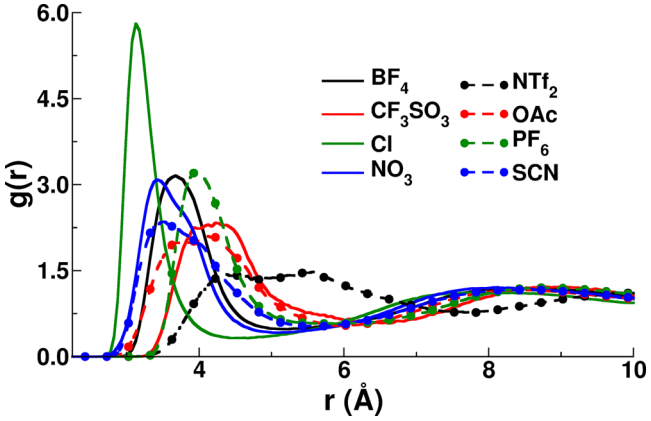

Figure 5. Radial distribution functions between COM (SO_2)–COM(anion) in SO_2–IL mixtures. $[BMIM]^+$ is common cation.

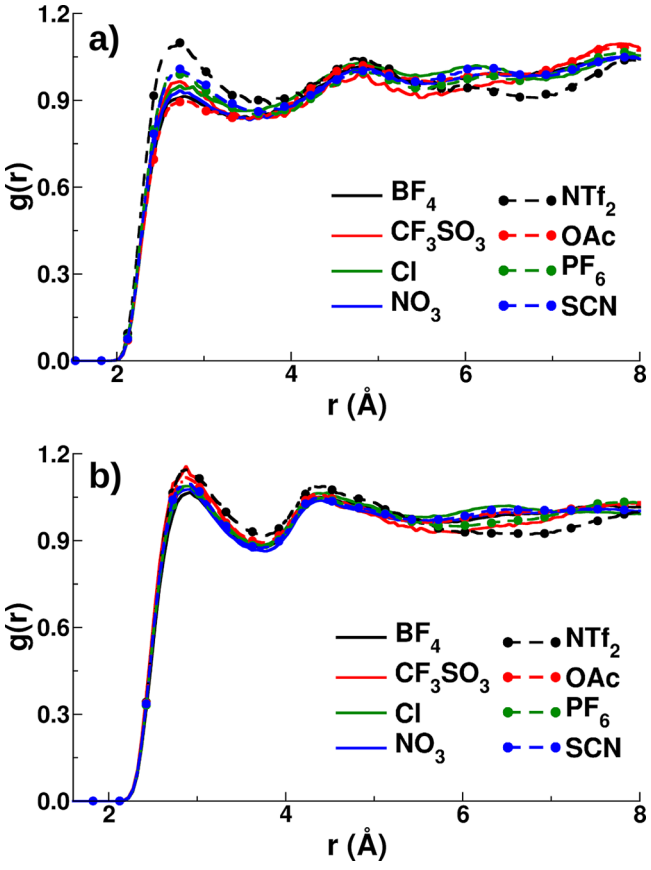

Figure 6. Radial distribution functions between (a) SO_2–H_B and (b) SO_2–H_1 in SO_2–IL mixtures. $[BMIM]^+$ is the common cation.

interaction with SO_2 (than H_A as is evident from the well-defined and sharp peak around 2.6–2.7 Å in Figure 6). The coordination numbers (integrated RDFs up to 3.5 Å) suggest that SO_2 molecule is surrounded by more H_1 atoms (1.65) than H_B atoms (0.75), which is consistent with the preference seen in gas phase quantum chemical calculations. Interestingly, the acidic hydrogen (H_A) atom having a strong interaction with anion (see Figure S3 of Supporting Information), also shows notable contact with SO_2, indicated by a sharp rise at short distance of 2.2 Å in Figure S4b, but its peak height is lower than that with either the H_B or H_1 (Figure 6). It is followed by a small hump at around 4.2 Å, and broad peak around 6 Å. On the contrary, the interaction of CO_2 with IL cation is primarily driven by the dispersion between solute and alkyl side chain, as no such direct contact between oxygen of CO_2 and the acidic hydrogen atom (H_A) on imidazolium ring was observed in a simulation of CO_2–IL solution (Figure S5 of Supporting Information) and in previous reports as well.[81,82] Thus, the considerably higher solubility of SO_2 than CO_2 in ILs might be a consequence of the crucial contrast in their structure of the solvation shell.

Spatial distribution functions (SDFs) were examined to validate these structural correlations. Figure 7 displays the computed SDFs of the anion and SO_2 molecule around the center of ring of the imidazolium cation, at isosurface values of 0.006 and 0.003 $Å^{-3}$, respectively. It is evident from Figure 7 that there is a hole in the density map of SO_2 exactly on top of the H_A atom. Instead, the density map of SO_2 is condensed around sites such as H_B and H_1, indicating binding preferences for SO_2 with these sites. Anions show stronger binding toward the most acidic hydrogen atom (H_A) located on the cation ring

DOI: 10.1021/acs.jpcb.6b02553
J. Phys. Chem. B 2016, 120, 4457–4466

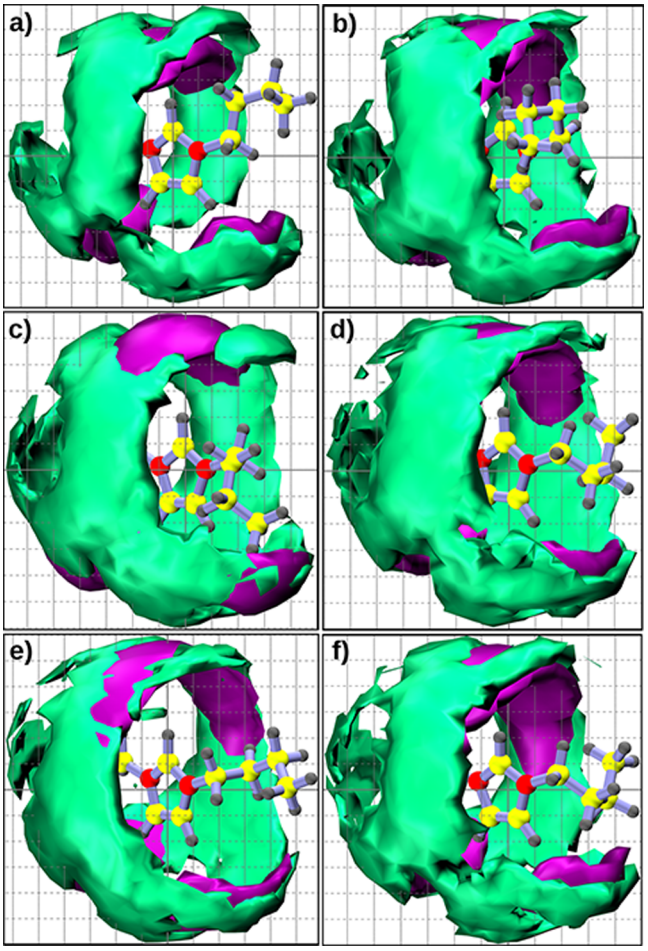

Figure 7. Spatial density map of anion (purple) and SO_2 (green) around the center of ring of the cation for (a) $[Cl]^-$, (b) $[NO_3]^-$, (c) $[OAc]^-$, (d) $[BF_4]^-$, (e) $[PF_6]^-$, and (f) $[SCN]^-$. Isosurface density: 0.006 $Å^{-3}$ (anion) and 0.003 $Å^{-3}$ (SO_2). Color scheme: red, nitrogen; yellow, carbon; gray, hydrogen.

(see anion density map in Figure 7) than the neutral SO_2 molecules do. Consequently, SO_2 interacts with the other hydrogen atoms on cation, i.e., H_B and H_1. These observations are in agreement with the RDF analysis and gas phase quantum chemical calculations. Spatial distributions of cation ring center and of SO_2 molecule around the center of mass of the anion are displayed in Figure 8. Although both cation and SO_2 share the same space around the anion, the latter interacts from a shorter distance than the former. A similar phenomenon was also observed in their respective radial distribution functions (see Figure S6 of Supporting Information). The more electron rich centers in anion e.g. oxygens of $[OAc]^-$, $[NO_3]^-$, $[TFO]^-$, etc. are more preferred over the other sites by the cation and SO_2.

In order to quantify the arrangement of the anion and SO_2 around the cation ring plane, combined distribution functions (CDFs) were calculated.[83,84] Figure 9 shows the same for [BMIM][Cl]–SO_2 (see Figure S7 of Supporting Information for such data for other ILs). As described earlier, the acidic hydrogen atom H_A exhibits pronounced interaction with the anion rather than with the SO_2 molecule. Figure 9a and c indicate that the probability for anions to be located closer to this acidic hydrogen and more linear to the C_R–H_A bond is higher than that for SO_2. Similar conclusions can be drawn for other anions as shown in Figure S7 of Supporting Information.

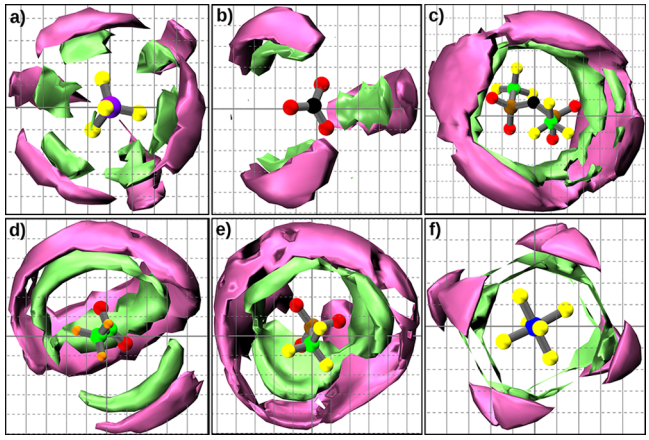

Figure 8. Spatial density map of cation (pink) and SO_2 (green) around the center of mass of the anion for (a) $[BF_4]^-$, (b) $[NO_3]^-$, (c) $[NTf_2]^-$, (d) $[OAc]^-$, (e) $[TFO]^-$, and (f) $[PF_6]^-$. Isosurfaces are at a density of 0.006 $Å^{-3}$ for the cation and 0.003 $Å^{-3}$ for SO_2. Color scheme: nitrogen, black; carbon, green; hydrogen, orange; oxygen, red; sulfur, ochre; boron, violet; fluorine, yellow; phosphorus, blue.

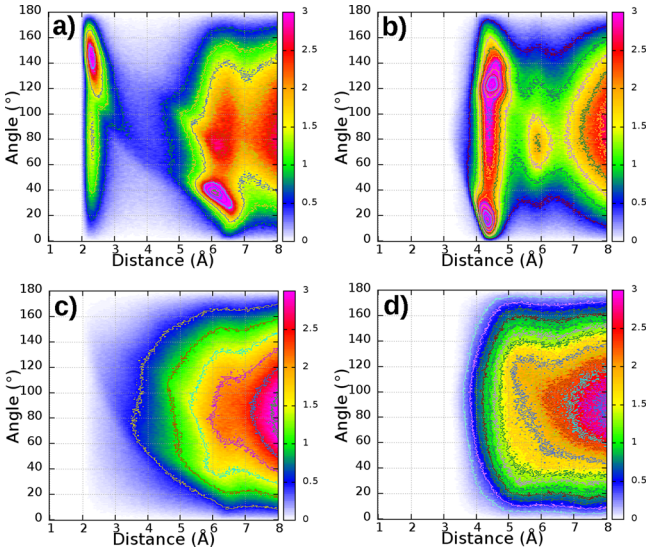

Figure 9. Combined distribution functions depicting the in-plane and on-top distribution with relative intensity color coding. The distance is (a) H_A–anion, (b) CoR–CoM (anion), (c) H_A–SO_2 and (d) CoR–CoM (SO_2), respectively. The angle is (a) C_R–H_A–anion, (b) CoR–C_R–CoM (anion), (c) C_R–H_A–SO_2 and (d) CoR–C_R–CoM (SO_2), respectively. CoR indicates the center of the imidazolium ring and CoM indicates the center of mass of either anion or of SO_2. The anion is chloride. Data for other ILs are displayed in Figure S7 of Supporting Information.

The CDFs depicting the coordination at acidic hydrogen atom reveal that the anion interacts directly toward the H_A atom (in-plane arrangement) and this directionality is most intense in [BMIM][Cl] and least in [BMIM][TFSO]. This trend can be justified based on the reduced acceptor probability due to larger charge delocalization in anions such as $[PF_6]^-$, $[TFSO]^-$ etc. However, the orientation of SO_2 molecule toward the acidic hydrogen atom is independent of the anion. It is evident from Figure 9b,d (also Figure S7 of Supporting Information) that the anion is likely to be present on-top of the imidazolium ring too at short distances when compared to that of SO_2 distribution. These observations further substantiate the fact that SO_2 is

DOI: 10.1021/acs.jpcb.6b02553
J. Phys. Chem. B 2016, 120, 4457–4466

more likely to be found near the methyl hydrogen atoms (H_1) which was also seen in RDF analysis and gas phase DFT calculations.

Thermodynamics of SO_2 Absorption. The potential of mean force (PMF) for bringing the solute, SO_2, from its vapor phase into the bulk IL was calculated. The free energy profiles for SO_2 solvation in various ILs consisting $[BMIM]^+$ as the common cation combined with different anions are displayed in Figure 10. Solvation free energy (SFE) is the difference in the

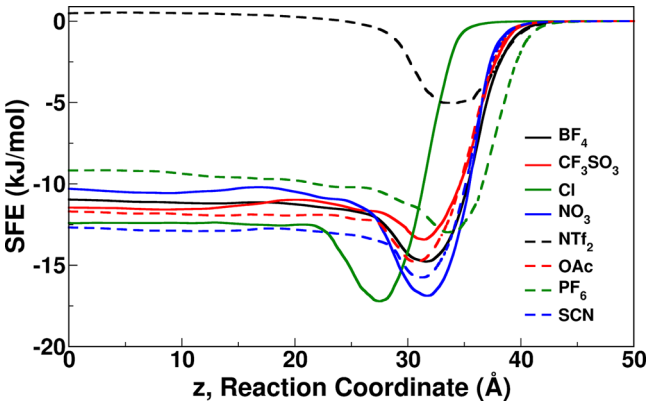

Figure 10. Solvation free energy profile of SO_2 in various ionic liquids ($[BMIM]^+$ as common cation). z = 0 is the center of mass of IL (bulk), and z > 45 is SO_2 in vapor phase.

free energies between the vapor phase and the solvated state of the solute in the IL. The SFE profiles become zero around 42 Å in most ILs, except in [BMIM][Cl]. This is due to the smaller thickness of the [BMIM][Cl] liquid slab (see Figure S8 of Supporting Information). As the SO_2 approaches the liquid region, the PMF displays a monotonic decay and it become most negative at the air−IL interface. The PMF increases in value in the bulk region, before converging to a constant value. Similar kinds of PMF profiles were observed in earlier gas absorption studies in ILs.[59,60] The occurrence of the minimum near the air−IL interface in the SO_2 PMF clearly reveals a preference for the solute to be at the interface. Further, Figure 11 presents the PMF along with the number density profile of various sites on cation and anion in [BMIM][NO_3] (see Figure S9 of Supporting Information for other ILs). It is evident that the minimum in SO_2 PMF coincides with the maximum in C_1

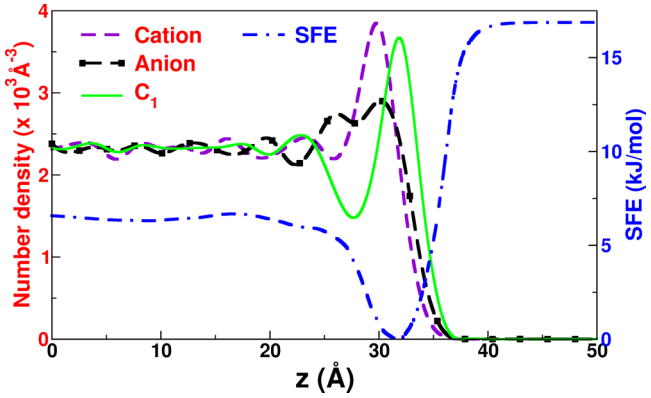

Figure 11. Number density profile of cation ring center, anion center of mass, and C_1 atom of butyl tail, compared against SO_2 PMF in [BMIM][NO_3].

number density at the interface, which confirms the preferable interaction of SO_2 with H_1 atoms over other sites of the cation. The cation alkyl chain is oriented normal to the liquid−vapor interface,[85] which can enhance the gas solubility through dispersion interaction with SO_2 (also seen from the bulk liquid structure). In addition, this may also lead to the formation of an adsorbed SO_2 layer at the interface, which indeed was found for CO_2 in a recent study.[86]

In a liquid system which is in equilibrium with its vapor phase, the change in potential energy across the vapor−liquid interface is presumed to be the same as the enthalpy change. Thus, the relative solubility of SO_2 in different ILs can be understood in terms of enthalpy and entropy contributions. The trend in SFE determined using an empirical force field can be correlated to the binding energy of one ion pair with a SO_2 molecule (computed at MP2/aug-cc-pVDZ level of theory) and a linear correlation is displayed in Figure 12. This observation

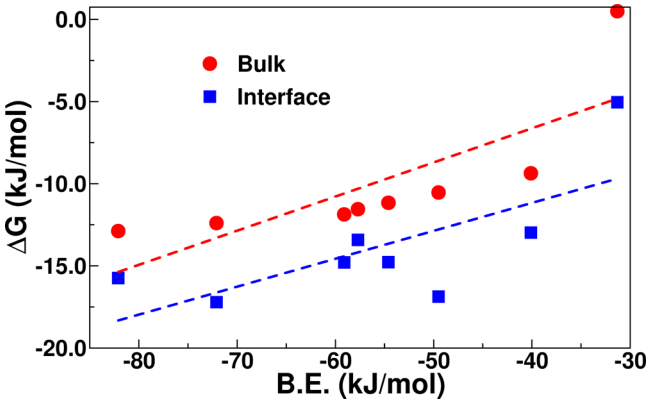

Figure 12. Binding energy (BE) of SO_2 with IL ion pair versus the solvation free energy (SFE) of SO_2 in bulk IL and in IL−vapor interface. BE is obtained from gas phase quantum chemical calculation while the SFE are determined from bulk MD simulations with an empirical force field. Dashed lines are best fits to data. Red (blue) circles are ΔG between SO_2 in vapor and in the bulk (interface) of IL.

suggests that the SO_2 solvation in ILs is largely enthalpy driven. In addition, the energetic and entropic contributions to SFE were determined through two additional simulations. In one, a solute SO_2 molecule was kept 40 Å away from the bulk IL region, i.e., clearly in the vapor phase. The other one contained the SO_2 molecule submerged inside the bulk IL. The simulation box dimensions, temperature etc. were kept the same as in those described in the Free Energy Calculation section. Both the systems were equilibrated in the *NVT* ensemble for 8 ns duration (see Figure S10 of the Supporting Information). The difference in potential energy between these two equilibrated systems was taken as the enthalpy change (ΔU) for SO_2 solvation. The entropy contribution to the dissolution process is obtained as the difference between the solvation free energy and the potential energy and the same is tabulated in Table 2. In most of the ILs, the change in entropy with respect to the energy difference is moderate. However, in the case of [BMIM][NTf_2], the relative entropy contribution is much higher than in rest of the ILs, resulting in it becoming a poor solvent for SO_2 solvation. Further investigation suggests that the addition of solute SO_2 in the bulk ionic liquids stretches the cation marginally (see Figure S11 of Supporting Information). For the smaller anions such as $[SCN]^-$, $[OAc]^-$, $[CF_3SO_3]^-$, $[BF_4]^-$, $[PF_6]^-$ etc. there is no conformational change and thus

DOI: 10.1021/acs.jpcb.6b02553
J. Phys. Chem. B 2016, 120, 4457−4466

Table 2. Changes in Free Energy ($\Delta G = G_{liq} - G_{gas}$), Enthalpy ($\Delta U = U_{liq} - U_{gas}$), and Entropy ($T\Delta S = S_{liq} - S_{gas}$) for SO_2 Solvation in Various ILs[a]

IL	ΔG (kJ/mol)	ΔU (kJ/mol)	$T\Delta S$ (kJ/mol)
$[SCN]^-$	−12.84	−53.68	−40.84
$[Cl]^-$	−12.38	−89.41	−77.03
$[OAc]^-$	−11.84	−75.35	−63.51
$[CF_3SO_3]^-$	−11.55	−35.23	−23.68
$[BF_4]^-$	−11.13	−81.46	−70.33
$[NO_3]^-$	−10.50	−60.21	−49.71
$[PF_6]^-$	−9.330	−59.99	−50.66
$[NTf_2]^-$	0.502	−43.89	−44.39

[a]ΔS is a derived quantity from ΔG and ΔU. $[BMIM]^+$ is the cation.

no change in geometry, upon addition of SO_2. However, $[NTf_2]^-$ being larger in size, can be rotationally excited and thus have different conformational preferences with and without SO_2. Figure 13 displays the distribution of distances

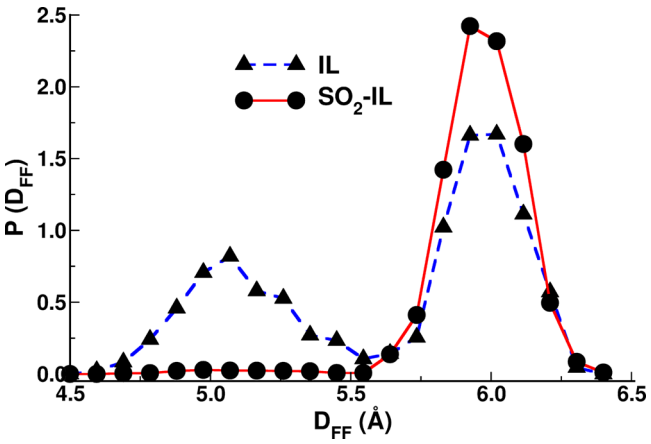

Figure 13. Distribution of distance between the terminal fluorine atoms of $[NTf_2]^-$ anion in pure $[BMIM][NTf_2]$ and in 50% SO_2 loaded $[BMIM][NTf_2]$ mixture.

between the terminal fluorine atoms in $[NTf_2]^-$ anion in pure $[BMIM][NTf_2]$ and in 50% SO_2 loaded $[BMIM][NTf_2]$. It is evident that the distribution becomes narrower on addition of SO_2 in bulk IL. The increased width of this distribution consequently expands its conformational space, increasing the entropy of SO_2 dissolved $[BMIM][NTf_2]$ and decreasing the free energy of dissolution. Among the ILs studied here, $[BMIM][SCN]$ appeared to be the best solvent for SO_2 capture, which is consistent with the experimental observation.[2]

The gas solubility in a liquid at infinite dilution can be measured via Henry's law constant, K_H. It is defined using the standard thermodynamic relation as

$$K_H = \frac{RT\rho}{M} \exp\left(\frac{\Delta G_{Sol}}{RT}\right) \quad (2)$$

where, ΔG_{Sol} is the free energy of solvation, ρ is the density, and M is the molecular weight of the pure IL. Henry's constant is indirectly proportional to gas solubility. The Henry's law constant of SO_2 in all the IL systems studied here is summarized in Table 3. Although there exists some differences in the solubility order reported in literature from simulations (e.g., solubility order, $[BMIM][NTf_2]$ > $[BMIM][BF_4]$ > $[BMIM][PF_6]$ by Elliott and co-workers[55] and $[BMIM][PF_6]$ > $[BMIM][NTf_2]$ > $[BMIM][BF_4]$ by Aparicio et al.[51]), we would like to discuss this matter in the light of our observations. As can be seen from Table 3, SO_2 is soluble in all ILs investigated here. The obtained K_H values showed the following solubility order:

$$[BMIM][SCN] > [BMIM][Cl] > [BMIM][OAc] > [BMIM][TFO] > [BMIM][BF_4] > [BMIM][NO_3] > [BMIM][PF_6] > [BMIM][NTf_2]$$

Thus, $[BMIM][SCN]$ is the most preferred solvent for SO_2 solvation, while $[BMIM][NTf_2]$ fares the worst. It is interesting to note that the solubility of SO_2 is more in ILs with smaller molar volumes.[55] Enthalpic contributions as captured through gas phase calculations and bulk MD simulations largely determine SO_2 solubility in ILs. These observations are important in further design of functional ionic liquids for SO_2 capture.

Table 3. Henry's Law Constant (K_H) of SO_2 in Studied ILs at 298 K and P = 1 atm

IL	K_H (atm)
$[BMIM][SCN]$	0.77
$[BMIM][Cl]$[a]	1.01
$[BMIM][OAc]$	1.09
$[BMIM][CF_3SO_3]$	1.21
$[BMIM][BF_4]$	1.49
$[BMIM][NO_3]$	2.08
$[BMIM][PF_6]$	2.80
$[BMIM][NTf_2]$	5.72

[a]The temperature is 353 K.

Dynamics in SO_2−IL Mixtures. Ion self-diffusion coefficients in pure IL and SO_2−IL mixtures are computed from mean square displacement (see Figure S12 of the Supporting Information) and are compared in Table 4. Ionic diffusion in SO_2−IL mixture is higher than in pure ILs, which was also seen in previous MD simulations.[53,56,58,61] Likewise, shear viscosity and ionic conductivity are affected by the dissolution of SO_2 in ILs. Computed viscosity and electrical conductivity are presented in Table 5. In accordance with both experimental and simulation results,[2,13,53,56,58] the dissolution of SO_2 reduces the viscosity and enhances the electrical conductivity of the liquid. The transport coefficient values obtained from Green−Kubo relations for ILs, $[BMIM][NTf_2]$ and $[BMIM][SCN]$ showed adequate agreement with experimental measurements

Table 4. Ion Self-diffusion Coefficients ($\times 10^{-7}$ cm^2 s^{-1}) in Pure IL and SO_2−IL Mixtures Calculated from Bulk Simulations at 298 K

	D_+		D_-		
IL	pure[a]	mix	pure[a]	mix	D_{SO_2}
$[BMIM][SCN]$	9.48	16.1	9.97	20.2	57.98
$[BMIM][OAc]$	1.27	4.23	1.32	4.43	24.59
$[BMIM][CF_3SO_3]$	2.08	3.52	1.41	2.85	22.65
$[BMIM][BF_4]$	2.30	7.89	1.83	7.92	34.26
$[BMIM][NO_3]$	1.65	6.24	1.51	5.04	27.62
$[BMIM][PF_6]$	1.05	4.80	0.74	4.17	33.79
$[BMIM][NTf_2]$	2.70	7.73	2.10	5.98	33.82

[a]The temperature is 300 K.

DOI: 10.1021/acs.jpcb.6b02553
J. Phys. Chem. B 2016, 120, 4457−4466

Table 5. Shear Viscosity, η (mPa·s) and Electrical Conductivity, σ (S·m^{-1}) in Pure IL and SO_2−IL Mixtures at 298 K

IL	η		σ	
	pure[a]	mix	pure[a]	mix
[BMIM][SCN]	35.20	14.05	0.62	1.34
[BMIM][OAc]	191.5	62.19	0.07	0.31
[BMIM][CF_3SO_3]	65.00	32.21	0.25	0.66
[BMIM][BF_4]	71.00	26.39	0.42	1.06
[BMIM][NO_3]	129.0	50.38	0.31	0.76
[BMIM][PF_6]	185.0	72.19	0.17	0.51
[BMIM][NTf_2]	42.00	18.27	0.29	0.79

[a]The temperature is 300 K.

available at low SO_2 loading.[2] Although SO_2 has been reported to be reactive with some ionic liquids,[10,28] its effect on the IL viscosity is unknown. However, the viscosity of ionic liquids increases drastically upon chemisorption of CO_2.[87,88] In the present work, we assume the physisorption of SO_2 in ILs and thus the viscosity of the solution decreases with respect to the neat IL.

CONCLUSIONS

A microscopic understanding behind the solvation of SO_2 is important to obtain in order to interpret its solubilities in different ionic liquids. In this contribution, we have employed molecular dynamics simulations and *ab initio* calculations to provide a detailed understanding of the dissolution of SO_2 in ionic liquids and consequent changes in their structure and transport coefficients.

Gas phase quantum chemical calculation results indicated the propensity of both the cation and anion to interact with the SO_2 molecule. Strong charge transfer interaction between the anion and SO_2 molecule was also observed. A linear correlation between the binding energy of SO_2 with the ion pair and the net charge transfer (primarily from the anion to the SO_2 molecule) evidenced the anion···SO_2 interaction as the major contribution in SO_2 capture in ILs. Binding energy values ranged from −31.38 kJ/mol ([BMIM][NTf_2]) to −82.19 kJ/mol ([BMIM][SCN]). Thus, $[SCN]^-$ emerged as the best anion to provide high SO_2 capture efficiency.[2]

Condensed phase MD simulations of SO_2−IL mixtures revealed the significant role of both cations and anions in the SO_2 dissolution process. SO_2 molecule was found to be surrounded by the cations through dispersion interaction, mainly with the alkyl group which leads to the formation of a "cation cage" around SO_2. On the other hand, less than a pair of anions were present within the first coordination shell of the solute. Thus, SO_2 shares favorable interactions with both the cation and the anion. The dynamical consequences of the dissolution of SO_2 in IL are the significant decrease in the shear viscosity and a resultant increase in diffusion coefficient and electrical conductivity.

The free energy profiles for SO_2 dissolution obtained from MD simulations demonstrate the preference for the solute to be located at the IL-vapor interface relative to the bulk liquid; the same can be rationalized from the richness of the cation alkyl groups at the interface. A nearly linear relationship between the solvation free energy and the gas phase binding energy of SO_2 with the ions is observed which points to the enthalpic nature of SO_2 dissolution in ILs. Thus, a good solvent for SO_2 capture must possess good hydrogen bond donor ability in the cation and a strong interaction with the anion. The calculated solubility order, based on the Henry's law constant of SO_2 in various ILs, indicates [BMIM][SCN] to be the best solvent for SO_2 dissolution, which was also reported earlier experimentally.[2]

ASSOCIATED CONTENT

Supporting Information

The Supporting Information is available free of charge on the ACS Publications website at DOI: 10.1021/acs.jpcb.6b02553.

Charge transfer in IL−SO_2 complexes, reaction coordinate for SFE calculations, minimum energy structures of IL−SO_2 complexes, RDFs, CDFs, coordination numbers, mass density profiles, potential energy of SO_2 in ILs, and MSDs(PDF)

AUTHOR INFORMATION

Corresponding Author

*(S.B.) E-mail: bala@jncasr.ac.in. Telephone: +91 (80) 2208 2808. Fax: +91 (80) 2208 2766.

Notes

The authors declare no competing financial interest.

ACKNOWLEDGMENTS

We thank DST for support. SB thanks Sheikh Saqr Laboratory, JNCASR for a senior fellowship. We thank the Centre for the Development of Advanced Computing, Bangalore, where a part of the computations were carried out.

REFERENCES

(1) Smith, S. J.; van Aardenne, J.; Klimont, Z.; Andres, R. J.; Volke, A.; Delgado Arias, S. Anthropogenic sulfur dioxide emissions: 1850−2005. *Atmos. Chem. Phys.* **2011**, *11*, 1101−1116.

(2) Xing, H.; Liao, C.; Yang, Q.; Veith, G. M.; Guo, B.; Sun, X.-G.; Ren, Q.; Hu, Y.-S.; Dai, S. Ambient Lithium-SO_2 Batteries with Ionic Liquids as Electrolytes. *Angew. Chem., Int. Ed.* **2014**, *53*, 2099−2103.

(3) Ratnakumar, B. V.; Smart, M. C.; Ewell, R. C.; Whitcanack, L. D.; Kindler, A.; Narayanan, S. R.; Surampudi, S. Potentiostatic Depassivation of Lithium-Sulfur Dioxide Batteries on Mars Exploration Rovers. *J. Electrochem. Soc.* **2007**, *154*, A715−A724.

(4) Paik, Y.; Osegovic, J. P.; Wang, F.; Bowden, W.; Grey, C. P. ^{2}H MAS NMR Studies of the Manganese Dioxide Tunnel Structures and Hydroxides Used as Cathode Materials in Primary Batteries. *J. Am. Chem. Soc.* **2001**, *123*, 9367−9377.

(5) Zhang, H.; Zhong, X.; Shaw, J. C.; Liu, L.; Huang, Y.; Duan, X. Very high energy density silicide-air primary batteries. *Energy Environ. Sci.* **2013**, *6*, 2621−2625.

(6) Kilroy, W. P.; Ebner, W.; Chua, D. L.; Venkatasetty, H. V. Investigation of Li/SO_2 Cell Chemistry and Hazards by Spectroscopy and Accelerating Rate Calorimetry. *J. Electrochem. Soc.* **1985**, *132*, 274−281.

(7) Dey, A. N.; Kuo, H. C.; Piliero, P.; Kallianidis, M. Inorganic Electrolyte Li/SO_2 Rechargeable System: Development of a Prototype Hermetic C Cell and Evaluation of Its Performance and Safety Characteristics. *J. Electrochem. Soc.* **1988**, *135*, 2115−2120.

(8) Zheng, Y.; Kiil, S.; Johnsson, J. E. Experimental investigation of a pilot-scale jet bubbling reactor for wet flue gas desulphurisation. *Chem. Eng. Sci.* **2003**, *58*, 4695−4703.

(9) Ma, X.; Kaneko, T.; Tashimo, T.; Yoshida, T.; Kato, K. Use of limestone for SO_2 removal from flue gas in the semidry FGD process with a powder-particle spouted bed. *Chem. Eng. Sci.* **2000**, *55*, 4643−4652.

(10) Wu, W.; Han, B.; Gao, H.; Liu, Z.; Jiang, T.; Huang, J. Desulfurization of Flue Gas: SO_2 Absorption by an Ionic Liquid. *Angew. Chem., Int. Ed.* **2004**, *43*, 2415−2417.

DOI: 10.1021/acs.jpcb.6b02553
J. Phys. Chem. B 2016, 120, 4457−4466

(11) Cui, G.; Wang, C.; Zheng, J.; Guo, Y.; Luo, X.; Li, H. Highly efficient SO_2 capture by dual functionalized ionic liquids through a combination of chemical and physical absorption. *Chem. Commun.* **2012**, *48*, 2633−2635.
(12) Huang, J.; Riisager, A.; Wasserscheid, P.; Fehrmann, R. Reversible physical absorption of SO_2 by ionic liquids. *Chem. Commun.* **2006**, *2006*, 4027−4029.
(13) Ren, S.; Hou, Y.; Wu, W.; Liu, Q.; Xiao, Y.; Chen, X. Properties of Ionic Liquids Absorbing SO_2 and the Mechanism of the Absorption. *J. Phys. Chem. B* **2010**, *114*, 2175−2179.
(14) Wang, C.; Luo, X.; Luo, H.; Jiang, D.-e.; Li, H.; Dai, S. Tuning the Basicity of Ionic Liquids for Equimolar CO_2 Capture. *Angew. Chem., Int. Ed.* **2011**, *50*, 4918−4922.
(15) Wang, C.; Luo, H.; Jiang, D.-e.; Li, H.; Dai, S. Carbon Dioxide Capture by Superbase-Derived Protic Ionic Liquids. *Angew. Chem., Int. Ed.* **2010**, *49*, 5978−5981.
(16) Bara, J. E.; Camper, D. E.; Gin, D. L.; Noble, R. D. Room-Temperature Ionic Liquids and Composite Materials: Platform Technologies for CO_2 Capture. *Acc. Chem. Res.* **2010**, *43*, 152−159.
(17) Bates, E. D.; Mayton, R. D.; Ntai, I.; Davis, J. H. CO_2 Capture by a Task-Specific Ionic Liquid. *J. Am. Chem. Soc.* **2002**, *124*, 926−927.
(18) Zhang, Y.; Zhang, S.; Lu, X.; Zhou, Q.; Fan, W.; Zhang, X. Dual Amino-Functionalised Phosphonium Ionic Liquids for CO_2 Capture. *Chem. - Eur. J.* **2009**, *15*, 3003−3011.
(19) Huang, J.-F.; Luo, H.; Liang, C.; Sun, I.; Baker, G. A.; Dai, S. Hydrophobic Brønsted Acid-Base Ionic Liquids Based on PAMAM Dendrimers with High Proton Conductivity and Blue Photoluminescence. *J. Am. Chem. Soc.* **2005**, *127*, 12784−12785.
(20) Merrigan, T. L.; Bates, E. D.; Dorman, S. C.; Davis, J. H., Jr. New fluorous ionic liquids function as surfactants in conventional room-temperature ionic liquids. *Chem. Commun.* **2000**, 2051−2052.
(21) Bara, J. E.; Carlisle, T. K.; Gabriel, C. J.; Camper, D.; Finotello, A.; Gin, D. L.; Noble, R. D. Guide to CO_2 Separations in Imidazolium-Based Room-Temperature Ionic Liquids. *Ind. Eng. Chem. Res.* **2009**, *48*, 2739−2751.
(22) Anderson, J. L.; Dixon, J. K.; Maginn, E. J.; Brennecke, J. F. Measurement of SO_2 Solubility in Ionic Liquids. *J. Phys. Chem. B* **2006**, *110*, 15059−15062.
(23) Shiflett, M. B.; Yokozeki, A. Separation of Carbon Dioxide and Sulfur Dioxide Using Room-Temperature Ionic Liquid [bmim]-[$MeSO_4$]. *Energy Fuels* **2010**, *24*, 1001−1008.
(24) Hong, S. Y.; Im, J.; Palgunadi, J.; Lee, S. D.; Lee, J. S.; Kim, H. S.; Cheong, M.; Jung, K.-D. Ether-functionalized ionic liquids as highly efficient SO_2 absorbents. *Energy Environ. Sci.* **2011**, *4*, 1802−1806.
(25) Boniface, J.; Shi, Q.; Li, Y. Q.; Cheung, J. L.; Rattigan, O. V.; Davidovits, P.; Worsnop, D. R.; Jayne, J. T.; Kolb, C. E. Uptake of Gas-Phase SO_2, H_2S, and CO_2 by Aqueous Solutions. *J. Phys. Chem. A* **2000**, *104*, 7502−7510.
(26) Yuan, X. L.; Zhang, S. J.; Lu, X. M. Hydroxyl Ammonium Ionic Liquids: Synthesis, Properties, and Solubility of SO_2. *J. Chem. Eng. Data* **2007**, *52*, 1150−1150.
(27) Yokozeki, A.; Shiflett, M. B. Separation of Carbon Dioxide and Sulfur Dioxide Gases Using Room-Temperature Ionic Liquid [hmim][Tf_2N]. *Energy Fuels* **2009**, *23*, 4701−4708.
(28) Shiflett, M. B.; Yokozeki, A. Chemical Absorption of Sulfur Dioxide in Room-Temperature Ionic Liquids. *Ind. Eng. Chem. Res.* **2010**, *49*, 1370−1377.
(29) Yang, D.; Hou, M.; Ning, H.; Ma, J.; Kang, X.; Zhang, J.; Han, B. Reversible Capture of SO_2 through Functionalized Ionic Liquids. *ChemSusChem* **2013**, *6*, 1191−1195.
(30) Shang, Y.; Li, H.; Zhang, S.; Xu, H.; Wang, Z.; Zhang, L.; Zhang, J. Guanidinium-based ionic liquids for sulfur dioxide sorption. *Chem. Eng. J.* **2011**, *175*, 324−329.
(31) Jiang, Y.-Y.; Zhou, Z.; Jiao, Z.; Li, L.; Wu, Y.-T.; Zhang, Z.-B. SO_2 Gas Separation Using Supported Ionic Liquid Membranes. *J. Phys. Chem. B* **2007**, *111*, 5058−5061.
(32) Luis, P.; Neves, L.; Afonso, C.; Coelhoso, I.; Crespo, J.; Garea, A.; Irabien, A. Facilitated transport of CO_2 and SO_2 through Supported Ionic Liquid Membranes (SILMs). *Desalination* **2009**, *245*, 485−493.
(33) Hu, X.-B.; Li, Y.-X.; Huang, K.; Ma, S.-L.; Yu, H.; Wu, Y.-T.; Zhang, Z.-B. Impact of α-d-glucose pentaacetate on the selective separation of CO_2 and SO_2 in supported ionic liquid membranes. *Green Chem.* **2012**, *14*, 1440−1446.
(34) Yang, Z.-Z.; He, L.-N.; Song, Q.-W.; Chen, K.-H.; Liu, A.-H.; Liu, X.-M. Highly efficient SO_2 absorption/activation and subsequent utilization by polyethylene glycol-functionalized Lewis basic ionic liquids. *Phys. Chem. Chem. Phys.* **2012**, *14*, 15832−15839.
(35) Wang, C.; Zheng, J.; Cui, G.; Luo, X.; Guo, Y.; Li, H. Highly efficient SO_2 capture through tuning the interaction between anion-functionalized ionic liquids and SO_2. *Chem. Commun.* **2013**, *49*, 1166−1168.
(36) Chen, K.; Lin, W.; Yu, X.; Luo, X.; Ding, F.; He, X.; Li, H.; Wang, C. Designing of anion-functionalized ionic liquids for efficient capture of SO_2 from flue gas. *AIChE J.* **2015**, *61*, 2028−2034.
(37) Wang, C.; Cui, G.; Luo, X.; Xu, Y.; Li, H.; Dai, S. Highly Efficient and Reversible SO_2 Capture by Tunable Azole-Based Ionic Liquids through Multiple-Site Chemical Absorption. *J. Am. Chem. Soc.* **2011**, *133*, 11916−11919.
(38) Cui, G.; Lin, W.; Ding, F.; Luo, X.; He, X.; Li, H.; Wang, C. Highly efficient SO_2 capture by phenyl-containing azole-based ionic liquids through multiple-site interactions. *Green Chem.* **2014**, *16*, 1211−1216.
(39) Wang, C.; Zheng, J.; Cui, G.; Luo, X.; Guo, Y.; Li, H. Highly efficient SO_2 capture through tuning the interaction between anion-functionalized ionic liquids and SO_2. *Chem. Commun.* **2013**, *49*, 1166−1168.
(40) Cui, G.; Zhang, F.; Zhou, X.; Li, H.; Wang, J.; Wang, C. Tuning the Basicity of Cyano-Containing Ionic Liquids to Improve SO_2 Capture through Cyano-Sulfur Interactions. *Chem. - Eur. J.* **2015**, *21*, 5632−5639.
(41) Lei, Z.; Dai, C.; Chen, B. Gas Solubility in Ionic Liquids. *Chem. Rev.* **2014**, *114*, 1289−1326.
(42) Cadena, C.; Anthony, J. L.; Shah, J. K.; Morrow, T. I.; Brennecke, J. F.; Maginn, E. J. Why Is CO_2 So Soluble in Imidazolium-Based Ionic Liquids? *J. Am. Chem. Soc.* **2004**, *126*, 5300−5308.
(43) Huang, X.; Margulis, C. J.; Li, Y.; Berne, B. J. Why Is the Partial Molar Volume of CO_2 So Small When Dissolved in a Room Temperature Ionic Liquid? Structure and Dynamics of CO_2 Dissolved in [Bmim] [PF_6]. *J. Am. Chem. Soc.* **2005**, *127*, 17842−17851.
(44) Bhargava, B. L.; Balasubramanian, S. Insights into the Structure and Dynamics of a Room-Temperature Ionic Liquid: Ab Initio Molecular Dynamics Simulation Studies of 1-n-Butyl-3-methylimidazolium Hexafluorophosphate ([bmim][PF_6]) and the [bmim][PF_6]−CO_2 Mixture. *J. Phys. Chem. B* **2007**, *111*, 4477−4487.
(45) Shah, J. K.; Maginn, E. J. Monte Carlo Simulations of Gas Solubility in the Ionic Liquid 1-n-Butyl-3-methylimidazolium Hexafluorophosphate. *J. Phys. Chem. B* **2005**, *109*, 10395−10405.
(46) Wang, Y.; Pan, H.; Li, H.; Wang, C. Force Field of the TMGL Ionic Liquid and the Solubility of SO_2 and CO_2 in the TMGL from Molecular Dynamics Simulation. *J. Phys. Chem. B* **2007**, *111*, 10461−10467.
(47) Bhargava, B. L.; Krishna, A. C.; Balasubramanian, S. Molecular dynamics simulation studies of CO_2−[bmim][PF_6] solutions: Effect of CO_2 concentration. *AIChE J.* **2008**, *54*, 2971−2978.
(48) Zhang, X.; Huo, F.; Liu, Z.; Wang, W.; Shi, W.; Maginn, E. J. Absorption of CO_2 in the Ionic Liquid 1-n-Hexyl-3-methylimidazolium Tris(pentafluoroethyl)trifluorophosphate ([hmim][FEP]): A Molecular View by Computer Simulations. *J. Phys. Chem. B* **2009**, *113*, 7591−7598.
(49) Deschamps, J.; Costa Gomes, M. F.; Pádua, A. A. H. Molecular Simulation Study of Interactions of Carbon Dioxide and Water with Ionic Liquids. *ChemPhysChem* **2004**, *5*, 1049−1052.
(50) Urukova, I.; Vorholz, J.; Maurer, G. Solubility of CO_2, CO, and H_2 in the Ionic Liquid [bmim][PF_6] from Monte Carlo Simulations. *J. Phys. Chem. B* **2005**, *109*, 12154−12159.

DOI: 10.1021/acs.jpcb.6b02553
J. Phys. Chem. B 2016, 120, 4457−4466

(51) Garcia, G.; Atilhan, M.; Aparicio, S. A density functional theory insight towards the rational design of ionic liquids for SO_2 capture. *Phys. Chem. Chem. Phys.* **2015**, *17*, 13559−13574.
(52) Zhang, X.; Liu, X.; Yao, X.; Zhang, S. Microscopic Structure, Interaction, and Properties of a Guanidinium-Based Ionic Liquid and Its Mixture with CO_2. *Ind. Eng. Chem. Res.* **2011**, *50*, 8323−8332.
(53) Monteiro, M. J.; Ando, R. A.; Siqueira, L. J. A.; Camilo, F. F.; Santos, P. S.; Ribeiro, M. C. C.; Torresi, R. M. Effect of SO_2 on the Transport Properties of an Imidazolium Ionic Liquid and Its Lithium Solution. *J. Phys. Chem. B* **2011**, *115*, 9662−9670.
(54) Yu, G.; Chen, X. SO_2 Capture by Guanidinium-Based Ionic Liquids: A Theoretical Study. *J. Phys. Chem. B* **2011**, *115*, 3466−3477.
(55) Ghobadi, A. F.; Taghikhani, V.; Elliott, J. R. Investigation on the Solubility of SO_2 and CO_2 in Imidazolium-Based Ionic Liquids Using NPT Monte Carlo Simulation. *J. Phys. Chem. B* **2011**, *115*, 13599−13607.
(56) Mohammadi, M.; Foroutan, M. Molecular investigation of SO_2 gas absorption by ionic liquids: Effects of anion type. *J. Mol. Liq.* **2014**, *193*, 60−68.
(57) Firaha, D.; Kavalchuk, M.; Kirchner, B. SO_2 Solvation in the 1-Ethyl-3-Methylimidazolium Thiocyanate Ionic Liquid by Incorporation into the Extended Cation-Anion Network. *J. Solution Chem.* **2015**, *44*, 838−849.
(58) Siqueira, L. J. A.; Ando, R. A.; Bazito, F. F. C.; Torresi, R. M.; Santos, P. S.; Ribeiro, M. C. C. Shielding of Ionic Interactions by Sulfur Dioxide in an Ionic Liquid. *J. Phys. Chem. B* **2008**, *112*, 6430−6435.
(59) Wick, C. D.; Chang, T.-M.; Dang, L. X. Molecular Mechanism of CO_2 and SO_2 Molecules Binding to the Air/Liquid Interface of 1-Butyl-3-methylimidazolium Tetrafluoroborate Ionic Liquid: A Molecular Dynamics Study with Polarizable Potential Models. *J. Phys. Chem. B* **2010**, *114*, 14965−14971.
(60) Dang, L. X.; Chang, T.-M. Molecular Mechanism of Gas Adsorption into Ionic Liquids: A Molecular Dynamics Study. *J. Phys. Chem. Lett.* **2012**, *3*, 175−181.
(61) Morganti, J. D.; Hoher, K.; Ribeiro, M. C. C.; Ando, R. A.; Siqueira, L. J. A. Molecular Dynamics Simulations of Acidic Gases at Interface of Quaternary Ammonium Ionic Liquids. *J. Phys. Chem. C* **2014**, *118*, 22012−22020.
(62) Prasad, B. R.; Senapati, S. Explaining the Differential Solubility of Flue Gas Components in Ionic Liquids from First-Principle Calculations. *J. Phys. Chem. B* **2009**, *113*, 4739−4743.
(63) Dennington, R.; Keith, T.; Millam, J. *GaussView Version 5.*; Semichem Inc.: Shawnee Mission, KS, 2009.
(64) Boys, S.; Bernardi, F. The calculation of small molecular interactions by the differences of separate total energies. Some procedures with reduced errors. *Mol. Phys.* **1970**, *19*, 553−566.
(65) Frisch, M. J.; Trucks, G. W.; Schlegel, H. B.; Scuseria, G. E.; Robb, M. A.; Cheeseman, J. R.; Scalmani, G.; Barone, V.; Mennucci, B. et al. *Gaussian 09*, Revision D.01; Gaussian Inc.: Wallingford CT, 2009.
(66) Manz, T. A.; Sholl, D. S. Chemically Meaningful Atomic Charges That Reproduce the Electrostatic Potential in Periodic and Nonperiodic Materials. *J. Chem. Theory Comput.* **2010**, *6*, 2455−2468.
(67) Manz, T. A.; Sholl, D. S. Improved Atoms-in-Molecule Charge Partitioning Functional for Simultaneously Reproducing the Electrostatic Potential and Chemical States in Periodic and Nonperiodic Materials. *J. Chem. Theory Comput.* **2012**, *8*, 2844−2867.
(68) Plimpton, S. Fast Parallel Algorithms for Short-Range Molecular Dynamics. *J. Comput. Phys.* **1995**, *117*, 1−19.
(69) Mondal, A.; Balasubramanian, S. Quantitative Prediction of Physical Properties of Imidazolium Based Room Temperature Ionic Liquids through Determination of Condensed Phase Site Charges: A Refined Force Field. *J. Phys. Chem. B* **2014**, *118*, 3409−3422.
(70) Mondal, A.; Balasubramanian, S. A Refined All-Atom Potential for Imidazolium-Based Room Temperature Ionic Liquids: Acetate, Dicyanamide, and Thiocyanate Anions. *J. Phys. Chem. B* **2015**, *119*, 11041−11051.
(71) Mondal, A.; Balasubramanian, S. A Molecular Dynamics Study of Collective Transport Properties of Imidazolium-Based Room-Temperature Ionic Liquids. *J. Chem. Eng. Data* **2014**, *59*, 3061−3068.
(72) Ketko, M. H.; Kamath, G.; Potoff, J. J. Development of an Optimized Intermolecular Potential for Sulfur Dioxide. *J. Phys. Chem. B* **2011**, *115*, 4949−4954.
(73) Nosé, S. A unified formulation of the constant temperature molecular dynamics methods. *J. Chem. Phys.* **1984**, *81*, 511−519.
(74) Hoover, W. G. Canonical dynamics: Equilibrium phase-space distributions. *Phys. Rev. A: At., Mol., Opt. Phys.* **1985**, *31*, 1695−1697.
(75) Martínez, L.; Andrade, R.; Birgin, E. G.; Martínez, J. M. PACKMOL: A package for building initial configurations for molecular dynamics simulations. *J. Comput. Chem.* **2009**, *30*, 2157−2164.
(76) Humphrey, W.; Dalke, A.; Schulten, K. VMD: Visual Molecular Dynamics. *J. Mol. Graphics* **1996**, *14*, 33−38.
(77) Mondal, A.; Balasubramanian, S. A Molecular Dynamics Study of Collective Transport Properties of Imidazolium-Based Room-Temperature Ionic Liquids. *J. Chem. Eng. Data* **2014**, *59*, 3061−3068.
(78) Fiorin, G.; Klein, M. L.; Hénin, J. Using collective variables to drive molecular dynamics simulations. *Mol. Phys.* **2013**, *111*, 3345−3362.
(79) Darve, E.; Rodríguez-Gómez, D.; Pohorille, A. Adaptive biasing force method for scalar and vector free energy calculations. *J. Chem. Phys.* **2008**, *128*, 144120.
(80) Zeng, S.; Gao, H.; Zhang, X.; Dong, H.; Zhang, X.; Zhang, S. Efficient and reversible capture of SO_2 by pyridinium-based ionic liquids. *Chem. Eng. J.* **2014**, *251*, 248−256.
(81) Hollóczki, O.; Kelemen, Z.; Könczöl, L.; Szieberth, D.; Nyulászi, L.; Stark, A.; Kirchner, B. Significant Cation Effects in Carbon Dioxide-Ionic Liquid Systems. *ChemPhysChem* **2013**, *14*, 315−320.
(82) Hollóczki, O.; Firaha, D. S.; Friedrich, J.; Brehm, M.; Cybik, R.; Wild, M.; Stark, A.; Kirchner, B. Carbene Formation in Ionic Liquids: Spontaneous, Induced, or Prohibited? *J. Phys. Chem. B* **2013**, *117*, 5898−5907.
(83) Malberg, F.; Hollóczki, O.; Thomas, M.; Kirchner, B. En route formation of ion pairs at the ionic liquid-vacuum interface. *Struct. Chem.* **2015**, *26*, 1343−1349.
(84) Weber, H.; Salanne, M.; Kirchner, B. Toward an Accurate Modeling of Ionic Liquid-TiO_2 Interfaces. *J. Phys. Chem. C* **2015**, *119*, 25260−25267.
(85) Bhargava, B. L.; Balasubramanian, S. Layering at an Ionic Liquid-Vapor Interface: A Molecular Dynamics Simulation Study of [bmim][PF_6]. *J. Am. Chem. Soc.* **2006**, *128*, 10073−10078.
(86) Perez-Blanco, M. E.; Maginn, E. J. Molecular Dynamics Simulations of Carbon Dioxide and Water at an Ionic Liquid Interface. *J. Phys. Chem. B* **2011**, *115*, 10488−10499.
(87) Zhang, J.; Zhang, S.; Dong, K.; Zhang, Y.; Shen, Y.; Lv, X. Supported Absorption of CO_2 by Tetrabutylphosphonium Amino Acid Ionic Liquids. *Chem. - Eur. J.* **2006**, *12*, 4021−4026.
(88) Goodrich, B. F.; de la Fuente, J. C.; Gurkan, B. E.; Zadigian, D. J.; Price, E. A.; Huang, Y.; Brennecke, J. F. Experimental Measurements of Amine-Functionalized Anion-Tethered Ionic Liquids with Carbon Dioxide. *Ind. Eng. Chem. Res.* **2011**, *50*, 111−118.

DOI: 10.1021/acs.jpcb.6b02553
J. Phys. Chem. B 2016, 120, 4457−4466